Engineering Solid Mechanics12 (2024) 409-422

Contents lists available at GrowingScience

Engineering Solid Mechanics

homepage: www.GrowingScience.com/esm

Dual boundary element method for comparative studies on fatigue crack growth models

Jairo A Mantilla[a*], Manuel Martínez[b], Diego F Villegas[b], Oscar Bohorquez[a] and Jorge G. Díaz[c]

[a]*Grupo de investigación en diseño y manufactura (DIMA), Universidad industrial de Santander, Colombia*
[b]*Grupo de investigación en energía y medio ambiente (GIEMA), Universidad industrial de Santander, Colombia*
[c]*Tecnológico de Monterrey, Escuela de Ciencias e Ingeniería, Guadalajara 45138, México*

A R T I C L E I N F O

Article history:
Received 12 January 2023
Accepted 1 May 2024
Available online
1 May 2024

Keywords:
Fracture mechanics
Stress intensity factor
Boundary element method
Fatigue crack growth
Finite element method

A B S T R A C T

Fatigue crack growth studies require models that accurately predict component life with low uncertainty. Despite the large number of proposed models, there is no clarity on their applicability, which justifies a comparative analysis between some of them. The dual boundary element method (DBEM) was applied for cracked bodies, whereby the stress intensity factors (SIF), the growth rate, and the number of cycles were computed. Three crack increment models were studied under constant amplitude fatigue loads: the Paris, the Klesnil-Lucas, and the Forman models. Results were validated with experimental literature and through the finite element method, indicating that each model represents a specific zone of the crack growth curve. Klesnil-Lucas model reproduces the region near the fracture threshold, Paris fits the controlled crack growth zone, whereas Forman's model recreates the unstable fracture zone, i.e., when the stress intensity factor approaches the material's fracture toughness. The J-integral with stress field decomposition gave errors below 0.8% for mode I. Results were similar for the propagation path and the number of cycles to those obtained with the finite element method, with errors of about 3% considering different K-equivalent approaches. Klesnil-Lucas accurately predicts the number of cycles with an error margin below 3%, considering the curved region in the growth rate at the propagation onset, while the Paris model becomes very conservative, predicting values up to 50% lower than experimental data. The Klesnil-Lukas model is advised for simulating the entire crack propagation.

1. Introduction

The classical design of mechanical components considers three main factors: the applied load, the geometry of the element and some physical properties. The computational model, the low operational reliability, and the required experimental tests lead to high safety factors for this approach; therefore, in high performance applications such as medical equipment and aerospace, a design scheme that provides higher confidence is required. Fracture mechanics emerges as an engineering discipline that studies the resistance of an element by adding a new variable to the analysis, that is, crack nucleation and propagation (Aliabadi, 1997). Based on such guidelines, a more reliable design is made, facilitating preventive decision making. The analysis of cracked elements can only be performed purely analytically for basic geometries with certain simplifications. The time and cost required for experimental setup makes it inefficient in typical applications, therefore, a computational analysis using numerical methods presents an alternative for solving general problems with defined geometry and mixed boundary conditions (Shlyannikov et al., 2021). There are several numerical methods used in fracture mechanics: among them, the finite element method (FEM) and the boundary element method (BEM). Portela (Santana & Portela, 2016a) pioneered the use of the boundary element method to study the coalescence of multiple cracks using the ligament yield criterion theory, Liu (Liu et al., 2020) analyzed fatigue crack propagation in pressurized pipe bends subjected to alternating bending using the finite element method, Mantilla (Mantilla et al., 2021) simulated the variation of stress intensity factor for the wedge splitting test using FEM, Shlyannikov (Shlyannikov et al., 2021) used FEM to analyze mixed mode (I + II) propagation in aviation engine compressor disk while Leite (Leite & Gomes, 2019) applied the dual boundary element method to simulate the same fracture mode. Some studies have considered a hybrid between the two methods, Citarella (Citarella et

* Corresponding author.
E-mail addresses: jairo2218051@correo.uis.edu.co (J. A. Mantilla)

ISSN 2291-8752 (Online) - ISSN 2291-8744 (Print)

doi: 10.5267/j.esm.2024.5.001

al., 2016) used a combined DBEM + FEM approach for crack propagation in a low pressure aeroengine turbine vane segment. Although both methods present numerical accurate solutions, the BEM is more suitable for this type of analysis (Sedmak, 2018), because it only discretizes the boundary and not the complete domain of the model (**Fig. 1**), facilitating the meshing algorithms, resulting in a lower order system of equations and, consequently, decreasing the computational time (Leite & Gomes, 2019; Price & Trevelyan, 2014a). On the other hand, the 2D simplification of a 3D cracked body might induce errors due to thickness strain variation (Gómez et al., 2024).

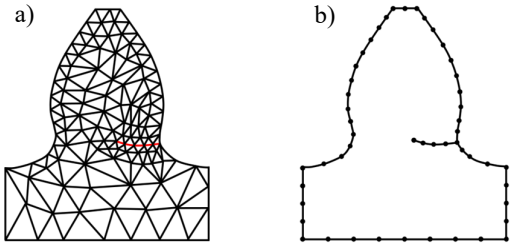

Fig. 1. Mesh comparison for cracked gear tooth using FEM and BEM. a) Finite element method, b) Boundary element method.

Simulating fatigue crack propagation phenomenon requires a mathematical model to predict the behavior of the material based on the crack growth curve, which relates the growth ratio (da/dN) to the variation of the applied stress intensity factor (ΔK) obtained experimentally. If there is mixed mode loading, a crack kinking criterion is also needed (Díaz & Freire, 2022). Several crack growth models have been reported in the literature (Machniewicz, 2013), some of which use the J-integral introduced by Rice (Rice, 1968) as the main parameter (Liu et al., 2020; Tanaka, 1983), others evaluate the energy release ratio (G) to estimate the propagation (Amsterdam et al., 2023), other use the crack opening displacement (Vaidya et al., 2010) and many models state that the growth ratio depends on the variation of the stress intensity factor (ΔK) when linear elastic conditions apply. It is useful to compare the estimation of growth ratios and component life with different stress intensity factors-based models. Therefore, a comparative analysis of three crack growth models under constant amplitude fatigue loading has been developed: the Paris-Erdogan (Paris & Erdogan, 1963), the Klesnil-Lucas (Klesnil & Lukáš, 1972) and the Forman models (Forman et al., 1967).

In this paper, the Dual Boundary Element Method (DBEM) with the J-integral has been applied to several problems for the simulation of cracked bodies under a plane (stress or strain) state, most of them restricted to fracture mode I for free traction cracks. The analysis contrasted the results of the growth ratios and number of cycles for each of the propagation models with experimental data from the three crack growth regions. The results obtained by the dual boundary element method were also used to validate the calculation of the stress intensity factor, the crack path, and the implementation of the models with other simulations, using the finite element method.

2. Materials and methods

The method of two-dimensional (2D) analysis of fatigue crack growth in homogeneous and isotropic materials includes firstly the overall simulation strategy and therefore the specific fundamentals of each operation performed during the simulation.

2.1 Overall simulation strategy

In the simulations performed, the process shown in **Fig. 2a** was carefully followed. With the initial conditions known, the DBEM with the J-integral was used to solve the mixed boundary problem and to calculate the stress intensity factors as the main result. Then, a cycle was run for each of the simulated increments. The maximum tangential stress (MTS) criterion was used to determine the crack growth direction (θ_t) and in this way the functional mesh can be modified as shown in **Fig. 2b**. DBEM is employed again to recalculate stresses, strains, displacements, and SIFs, initially and at the end of each increment. Once the calculation cycle was complete, one of the fatigue crack growth models was used to integrate the number of elapsed cycles and to locate the next point on the crack growth plot.

2.2 Dual Boundary Element Method (DBEM)

Table 1 compares some features between the DBEM and the finite element method (FEM) that support the use of DBEM in the current work, however, the main feature that makes the boundary element method particularly useful in the analysis of cracked bodies and crack growth is the model discretization (**Fig. 1**). For the computational crack growth analysis with DBEM, only new elements must be added in the growth direction (Wen & Aliabadi, 2012), whereas with the finite element method the whole domain, or at least a large part of it, must be re-meshed, which simplifies the meshing algorithms in the pre-processing and reduces the computation time. Since the general topology of the mesh remains unchanged, only new rows and columns are added to the system of equations used in the previous increment (Leite & Gomes, 2019; Price & Trevelyan, 2014b; Santana & Portela, 2016b).

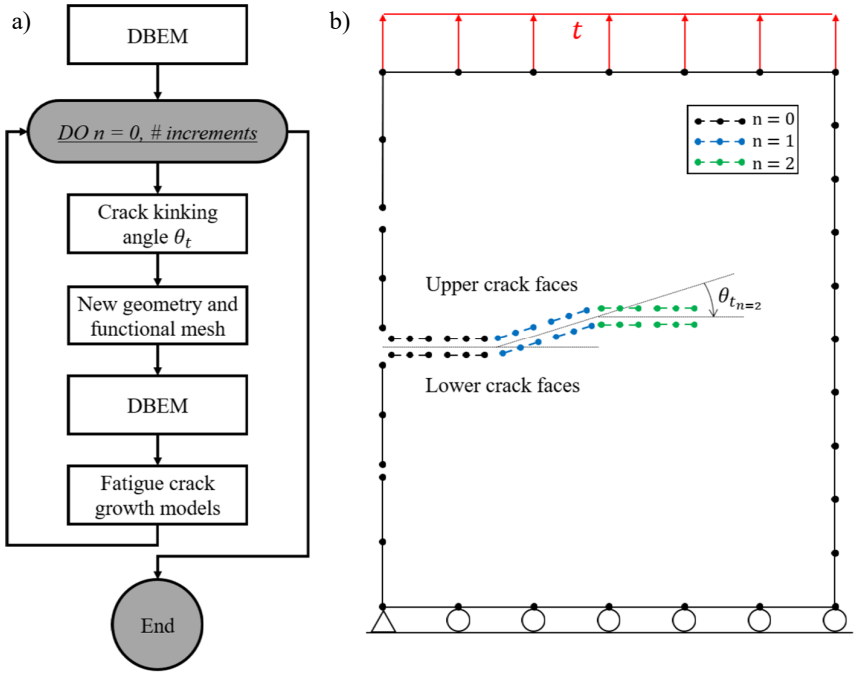

Fig. 2. General methodology for crack growth simulations. a) General flow diagram, b) Example of discretization showing the change in the functional mesh for the first two simulated increments.

Table 1. A comparison between DBEM and FEM algorithms.

Feature	**DBEM**	**FEM**
Discretization	Boundary (Γ)	Domain (Ω)
Computing time	Short	Time – consuming
Elements dimensionality	One dimension lower than the problem	Same problem dimension
Solution and results	Boundary calculation, postprocessing for internal points	Domain computation (all nodes)

The formulation of the boundary integral equations for two-dimensional (2D) elasticity in homogeneous isotropic materials with linear behavior is based on the Somigliana identity (Portela et al., 1993). This expression (1) allows the calculation of stresses and displacements in an internal point $\mathbf{x}'\epsilon\,\Omega$, by integrating the tractions and displacements at every boundary node $\mathbf{x}\,\epsilon\,\Gamma$ (**Fig. 3b**).

$$u_i(\mathbf{x}') + \int_\Gamma T_{ij}(\mathbf{x}'.\mathbf{x})u_j(\mathbf{x})d\Gamma(\mathbf{x}) = \int_\Gamma U_{ij}(\mathbf{x}'.\mathbf{x})t_j(\mathbf{x})d\Gamma(\mathbf{x}) \tag{1}$$

where $u_i(\mathbf{x}')$ is the displacement in the i-direction for the point of interest $\mathbf{x}'$, $u_j(\mathbf{x})$ and $t_j(\mathbf{x})$ are the displacement and traction in the j-direction at $\mathbf{x}\,\epsilon\,\Gamma$. The terms $T_{ij}(\mathbf{x}',\mathbf{x})$ and $U_{ij}(\mathbf{x}',\mathbf{x})$ represent the Kelvin fundamental solutions (Balderrama et al., 2006).

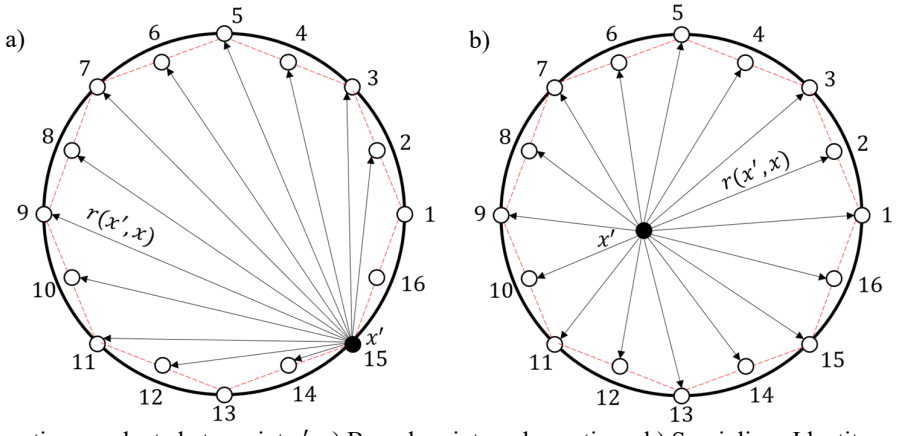

Fig. 3. Integral equations evaluated at a point x′. a) Boundary integral equations. b) Somigliana Identity.

The conventional boundary element method, just defined by the displacement equation, is indeterminate for cracked bodies, i.e., coincident boundaries on the crack faces (Leite & Gomes, 2019; Price & Trevelyan, 2014b). Consequently, the dual boundary elements method was used, made up of two independent equations (Wen & Aliabadi, 2012). The displacement Eq. (2) and the traction Eq. (3).

$$C_{ij}(\mathbf{x}')u_j(\mathbf{x}') + \int_\Gamma T_{ij}(\mathbf{x}'.\mathbf{x})u_j(\mathbf{x})d\Gamma(\mathbf{x}) = \int_\Gamma U_{ij}(\mathbf{x}'.\mathbf{x})t_j(\mathbf{x})d\Gamma(\mathbf{x}) \quad (2)$$

$$\frac{1}{2}t_j(\mathbf{x}') + n_i(\mathbf{x}')\int_\Gamma S_{kij}(\mathbf{x}'.\mathbf{x})u_k(\mathbf{x})d\Gamma(\mathbf{x}) = n_i(\mathbf{x}')\int_\Gamma D_{kij}(\mathbf{x}'.\mathbf{x})t_k(\mathbf{x})d\Gamma(\mathbf{x}) \quad (3)$$

where $C_{ij}(\mathbf{x}') = \delta_{ij}/2$ for a smooth boundary and $n_i(\mathbf{x}')$ is the normal to the boundary in the i-direction. $S_{kij}(\mathbf{x}', \mathbf{x})$ and $D_{kij}(\mathbf{x}', \mathbf{x})$ contain the derivatives of the fundamental solutions $T_{ij}(\mathbf{x}', \mathbf{x})$ and $U_{ij}(\mathbf{x}', \mathbf{x})$, respectively.

The boundary integral equations (2 and 3) were applied on the boundary discretization nodes $x' \epsilon\, \Gamma$ by evaluating the integrals throughout the boundary (Figure 3a), this involves dealing with different types of singularity cases during the integration of the element containing the application node $\mathbf{x}'$, a $1/r$ strong singularity in $T_{ij}(\mathbf{x}', \mathbf{x})$ and $D_{kij}(\mathbf{x}', \mathbf{x})$, a $\ln(1/r)$ soft singularity in $U_{ij}(\mathbf{x}', \mathbf{x})$ and a $1/r^2$ hyper singularity in $S_{kij}(\mathbf{x}', \mathbf{x})$ (Price & Trevelyan, 2014b). The displacement integral Eq. (2) was used on one of the crack faces and the traction integral Eq. (3) on the geometrically coincident opposite face. The displacement integral equation was applied for the rest of the boundary (**Fig. 4**).

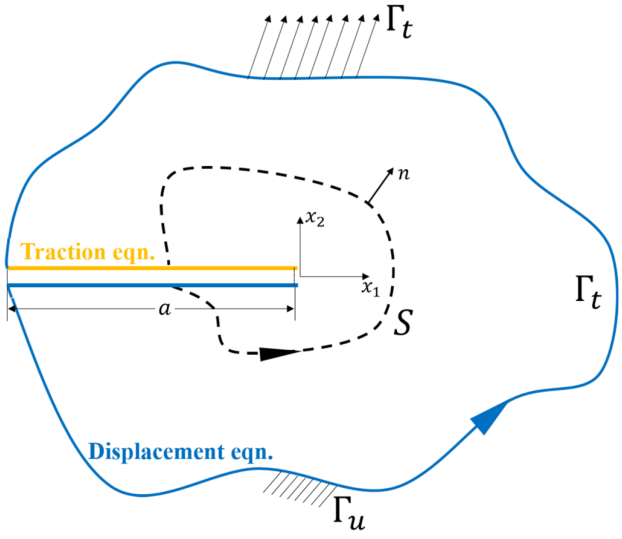

Fig. 4. A general sketch of the cracked body under mixed boundary conditions. The boundary integral equations approach is shown. The tractions and displacements are known in Γ_t and Γ_u, respectively. The J-integral was computed on an arbitrary contour S around the crack tip.

To solve all the tractions and displacements at the boundary, the method consists of first use Eq. (2) and Eq. (3) to solve the boundary and then apply the Somigliana identity (1) in the internal points required for the J integral evaluation and the stress intensity factor calculation. The cracked body was discretized completely with quadratic elements, the faces of the crack and the surrounding elements were discretized with discontinuous quadratic elements to work the singular and hyper singular integrals under the concept of Cauchy and Hadamard (Kats & Katz, 2019), the rest of the boundary was meshed with continuous elements.

2.3 J Integral

For the calculation of the stress intensity factors, the J integral was computed. The J integral is equal to the energy release rate for a body without volumetric forces (Rice, 1968). Eq. (4) illustrates the expression of the J-integral and its equivalence to the stress intensity factors in the case of linear elastic behavior.

$$J = \int_S (W n_1 - t_j u_{j.1})dS = \frac{1}{E'}(K_I^2 + K_{II}^2) \quad (4)$$

where W is the strain energy density, S is an arbitrary path around the crack tip (Fig. 4), n_1 is the normal vector to the integration path in direction 1, t_j is the traction vector, $u_{j,1}$ is the displacement, $E' = E$ for plane stress and $E' = E/(1-\nu^2)$ for plane strain and ν is the Poisson's ratio.

For each simulated increment, two elements (6 functional nodes) were added on each crack face in the growth direction, to define the local coordinate system x_1, x_2 (**Fig. 4**). The J-integral (4) was evaluated for a circular path around the crack tip made up of thirty-two internal points where the radius of the circle is defined as the distance from the crack tip to the fifth closest functional node. To decouple the SIFs, the elastic field is decomposed into the symmetric and the antisymmetric components (Liu et al., 2020). The J-integral was calculated using the trapezium rule with constant elements; however, it can be used with quadratic elements or even without contour discretization via Gauss-Legendre quadrature (Peixoto et al., 2023). This approach has been used with finite elements (Wang et al., 2023), boundary elements and experimentally using DIC to calculate stress intensity factors (Koko et al., 2020), as well as to establish the da/dN growth ratio as a function of ΔJ for materials with elastoplastic behavior (Tanaka, 1983; Xu et al., 2022).

2.4 Crack growth path

Based on the Westergaard elastic stress field solutions (Gdoutos, 1990), the maximum shear stress criterion was proposed and postulates that the crack grows in a direction perpendicular to the maximum tangential stress (MTS). This criterion was selected since the growth direction only depends on the ratio between the stress intensity factors K_I/K_{II} given by expression (5) and has proved to fit accurately in the implementation (Malíková et al., 2016; Wang et al., 2023).

$$\tan\left(\frac{\theta_t}{2}\right) = \frac{1}{4}\left(\frac{K_I}{K_{II}} \pm \sqrt{\left(\frac{K_I}{K_{II}}\right)^2 + 8}\right) \tag{5}$$

where θ_t refers to the growth angle measured from the local coordinate system at the crack tip (Figure 4). Two growth angles are available from expression (5), however, is chosen the one that produces the maximum principal stress in an equivalent I-mode (6).

$$K_{Ieq} = K_I \cos^3\left(\frac{\theta_t}{2}\right) - 3K_{II}\cos^2\left(\frac{\theta_t}{2}\right)\sin\left(\frac{\theta_t}{2}\right) \tag{6}$$

2.5 Fatigue crack growth models

Three fatigue crack propagation models were analyzed where the growth rate is related to the applied stress intensity factors.

2.5.1 Paris-Erdogan model (Paris & Erdogan, 1963):

$$\frac{da}{dN} = C(\Delta K)^m \tag{7}$$

2.5.2 Klesnil-Lucas model (Klesnil & Lukáš, 1972):

$$\frac{da}{dN} = C * (\Delta K^m - \Delta K_{th}^m) \tag{8}$$

2.5.3 Forman model (Forman et al., 1967):

$$\frac{da}{dN} = \frac{C(\Delta K)^m}{(1-R)K_{IC} - \Delta K} \tag{9}$$

where da/dN denote the crack growth rate, R is the fatigue load ratio, ΔK is the stress intensity factor variation, C and m are material-dependent experimental constants, ΔK_{th} and K_{IC} are the fracture threshold and the fracture toughness, respectively.

For the stress intensity factor variation (ΔK) in the crack growth models, the expression (10) postulated by Tanaka (Tanaka, 1974) was applied. Tanaka (10) works with two-dimensional problems in terms of an equivalent SIF variation (ΔK_{eq}) as a function of ΔK_I and ΔK_{II} for the opening and sliding shear loading modes, respectively. Sajith (Sajith et al., 2020) found Tanaka's model gives the closest fit to experimental results by comparing various equations of ΔK_{eq} for mixed mode in AISI 316 austenitic stainless Steel, Gómez (Gómez et al., 2024) found Tanaka's model best fits the experimental behavior of low-carbon steel under mixed mode and Shukla (Shukla & Murthy, 2023) showed that using the mixed mode Paris constants along with Tanaka's ΔK_{eq} model accurately and consistently predicts the fatigue life in Al 7075-T6 alloy.

$$\Delta K_{eq} = (\Delta K_I^2 + 2\Delta K_{II}^2)^{1/2} \tag{10}$$

Once the variation of the equivalent stress intensity factor was known, the simple trapezoid rule was used to integrate the number of elapsed cycles for each increment. A summary of the performed simulations is shown in **Table 2**.

Table 2. Summary of applied problems

Type of sample	Reference	Reference method	Fracture mode	Crack growth models
SENT	Zhu (Zhu, 2017) Shen (Shen et al., 2009) Bassindale (Bassindale et al., 2018)	Experimental FEM	Pure mode I	Paris
Rectangular Notch Plate (RNP)	Singh (Singh et al., 2011)	Experimental		Paris Klesnil-Lucas Forman
Compact tension (CT) in 7075 aluminum alloy	Zhao (Zhao et al., 2008) Newman (Newman et al., 2014)			
Perforated plate (PP)	Boljanovic (Boljanović & Maksimović, 2011) Sajith (Sajith et al., 2019)	Experimental FEM	Mixed mode (I + II)	Paris

3. Results and discussion

A simulation performed to validate the dual boundary element method and the J-integral is first presented, followed by comparative tests of the propagation models.

3.1 Single Edge Notched Test (SENT)

To validate the results of the stress intensity factors measured by DBEM, the simulation of the SENT test adopted by the BS 8571 standard to determine fracture toughness and the crack growth ratios in metals was conducted (Moore & Pisarski, 2017). This test is an alternative to those adopted in the American society with the Compact Tension (CT) and the Single Edge Notched Bending (SENB) specimens (Sajuri et al., 2011). The test involves the fracture of a specimen with the dimensions shown in **Fig. 5a**, subjected to an axial load P at both ends. According to the recommendation of the standard, $H/w = 10$ and $H^*/w = 4$ were used, where H is the clear length and H^* is the clamping length at each end, the thickness B is equal to the width w.

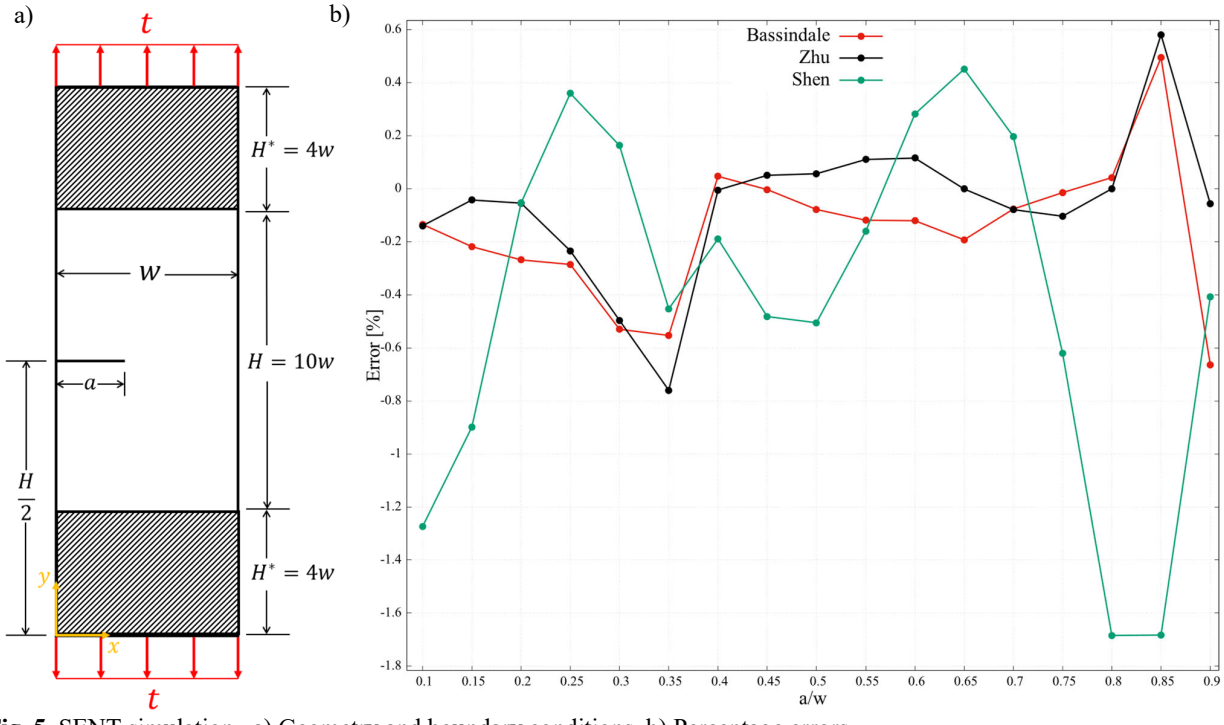

Fig. 5. SENT simulation. a) Geometry and boundary conditions, b) Percentage errors.

The SIF were compared with three references. The expression given by Zhu (Zhu, 2017) obtained from experimental correlations for pure tension and bending, the correlation of Shen (Shen et al., 2009) by simulation fitting and the Bassindale approach (Bassindale et al., 2018) through the finite element method from ABAQUS (Dassault Systèmes, Vélizy-Villacoublay, France). Crack lengths were varied from $a/w = 0.1$ to $a/w = 0.9$ with 0.05 increments, range in which the models were calibrated in the references.

Errors (**Fig. 5b**) of less than 1.7 % were obtained throughout the study range, in standard recommended range of $0.2 \leq a/w \leq 0.7$ the errors were less than 0.8 % that is in the absence of plasticity effects.

3.2 Rectangular Notched Probe (RNP)

The experimental test performed by Singh (Singh et al., 2011) on nano twinned copper was simulated with the specimen shown in **Fig. 6**. The material properties as well as general simulation parameters are presented in **Table 3**.

Table 3. RNP simulation parameters

Feature	Description	Feature	Description	Feature	Description
Problem type	Plane stress	Applied traction	135.9MPa, R=0.1	Poisson (υ)	0.34
Fracture toughness ($\mathbf{K_{IC}}$)	22.3 MPa$\sqrt{m}$	Elastic modulus	207 GPa	Fracture threshold (ΔK_{th})	5 MPa $\sqrt{m}$

The growth analysis was run from an initial crack size $a_i = 1.36$ mm to $a_f = 5.057$ mm, for a growth length $\Delta a = 3.697$ mm. The crack was discretized with elements of length $L_{elem} = 0.045$ mm, therefore, the growth length is achieved by running forty-one increments of twice the element length at the crack tip.

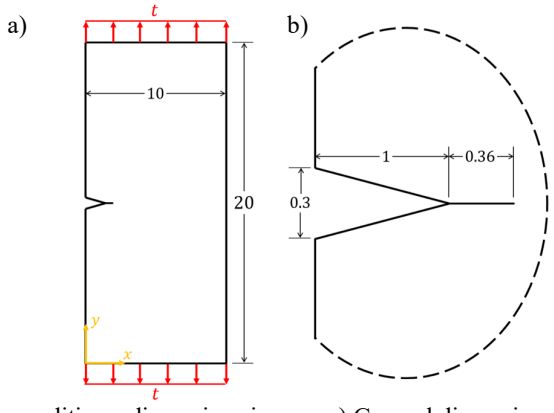

Fig. 6. Geometry and boundary conditions, dimensions in mm. a) General dimensions, b) Notch dimensions.

The initial geometric mesh contains 216 elements with 432 nodes, adding 4 new elements for each increment. Due to the loading conditions only mode I is dominantly present when the stress intensity factors were calculated (**Fig. 7a**). The stress intensity factor for mode II is almost zero, making $K_{eq} \approx K_I$. In consequence, crack propagation follows perpendicular to the applied load (**Fig. 7b**), consistent with experimental data (Singh et al., 2011).

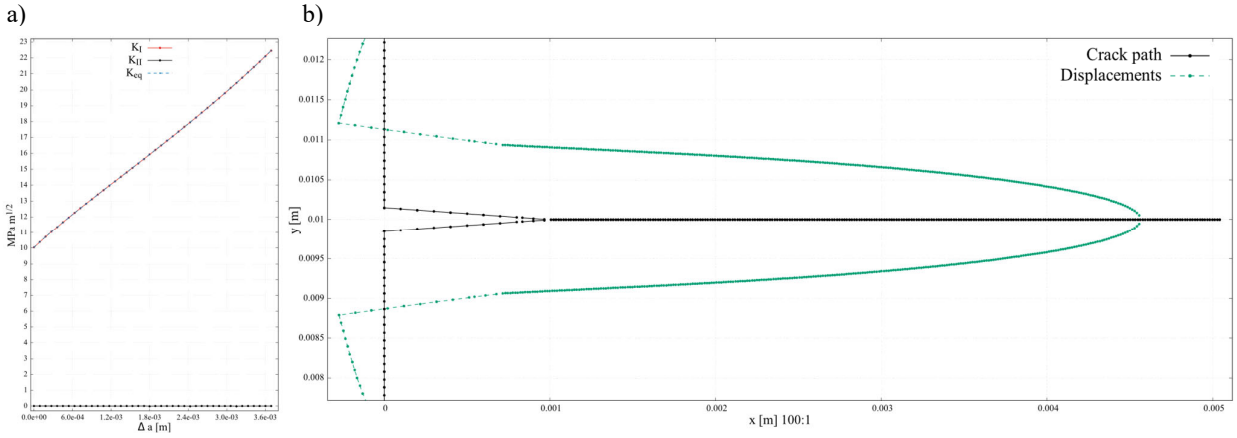

Fig. 7. Stress intensity factors and propagation path for RNP simulation. Scale for displacements 100:1.

For the Paris Erdogan model and the Klesnil Lucas model, $C = 1.1049 \times 10^{-12}$ and $m = 3.7719$ were used as growth constants, while for the Forman model $C = 6.0490 \times 10^{-10}$ and $m = 2.1719$. These constants were adjusted to the experimental data using the MATLAB optimization toolbox (MathWorks Inc., Massachusetts, USA). The crack growth plot and the number of elapsed cycles is presented in Figure 8.

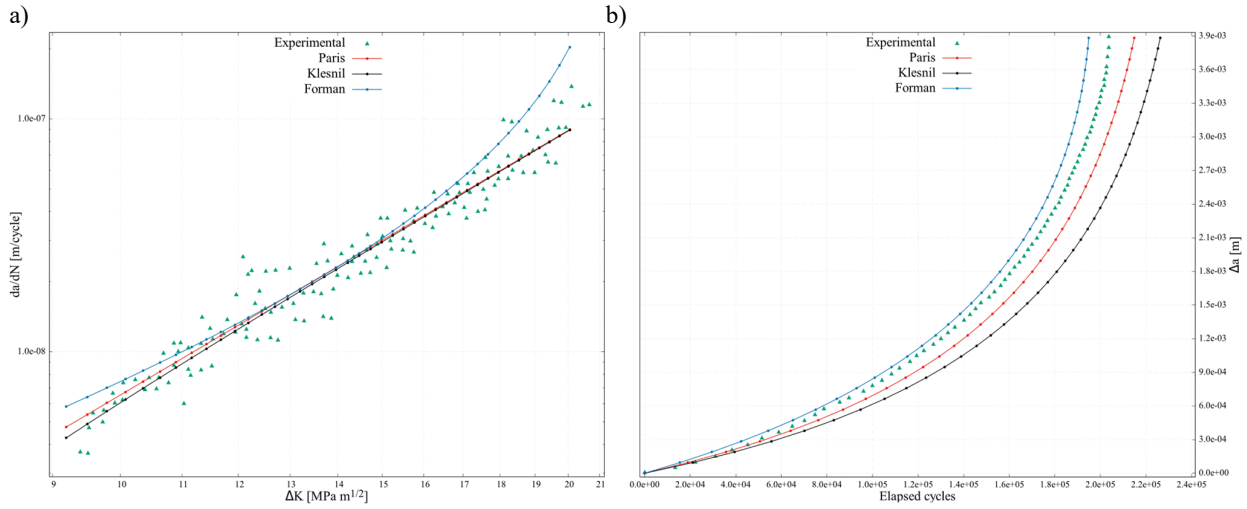

Fig. 8. Numerical vs. experimental results (Singh et al., 2011) comparison for RNP simulation. a) Crack growth plot, b) Crack size vs. number of cycles.

The experimental test (Singh et al., 2011) only presents results for crack growth in part of zone II and zone III. No data are available for zone I, so the estimation of the fracture threshold was done with considerable uncertainty. The Paris-Erdogan model represents a straight line in the growth graph; therefore, it assumes no deviation from the linear behavior of zone II. The Forman model, which includes fracture toughness, reproduces the fast and uncontrolled crack growth, i.e., the final part of zone II and zone III until total failure. Klesnil-Lucas presents a curve that resembles the Paris line for high growth rates ($> 2 \times 10^{-8}$ m/cycle) away from slow crack propagation.

The Paris-Erdogan model, which best fits the experimental data in **Fig. 8a**, accurately estimates the number of cycles for this specific case (**Fig. 8b**). However, the three models do not have notable differences in the lifetime estimation, this is because they are only considering zones II and III of the growth. The fast growth region represents a very small percentage of the total number of cycles, and for this reason, although the Forman model takes it into account, it is recognized that it has no applicability in engineering terms, since life cycle analysis is the main objective in the design of a component. In the following simulation the propagation is analyzed when the slow growing region I is included.

3.3 Crack growth in 7075 - T651 aluminum alloy

The simulation reproduces the experimental test performed by Zhao (Zhao et al., 2008) based on ASTM E647 (ASTM, 2023), by controlled fracture of the compact tension specimen with the dimensions shown in **Fig. 9**. A maximum load of P_{max} = 1.6 kN was applied with a fatigue load ratio R = 0.1. The test starts with a crack size a_i = 7.3 mm up to a_f = 34.3 mm, noting that the last one does not correspond to the final fracture of the specimen. 54 increments of 0.5 mm were simulated to achieve a total variation of Δa = 27 mm.

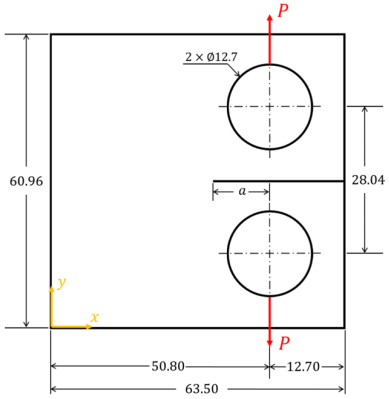

Fig. 9. Compact tension geometry based on ASTM E647 (ASTM, 2023), dimensions in mm.

The mechanical properties used were E = 71100 MPa and v = 0.33 (Mukherjee et al., 2015). Crack growth was simulated using the Klesnil-Lucas and Paris-Erdogan models with $C^* = 8.3399 \times 10^{-11}$, $m^* = 3.5$ and $\Delta K^*_{th} = 4.58$ MPa$\sqrt{m}$.

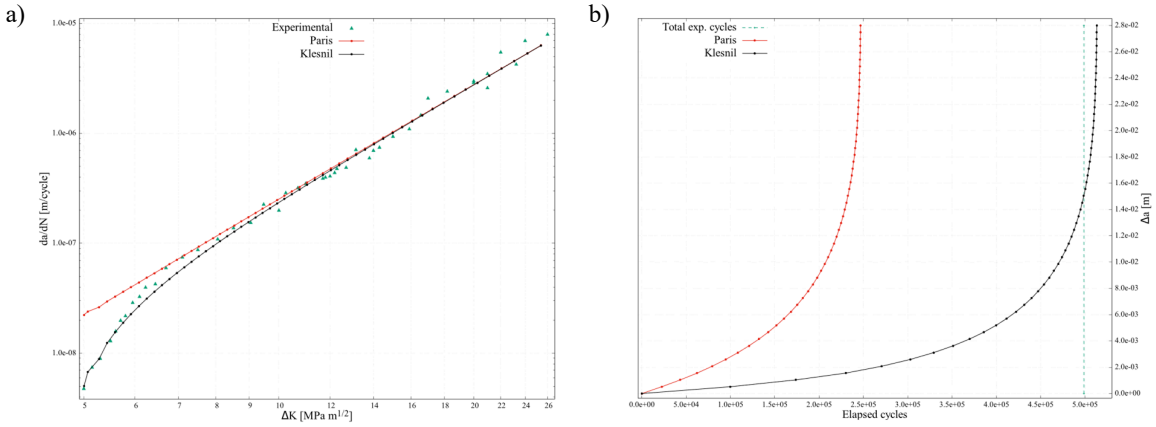

Fig. 10. Numerical vs. experimental reference (Zhao et al., 2008) comparison for crack growth in 7075 – T651 alloy. a) Crack growth plot, b) Crack size vs. number of cycles.

When part of region I is experimentally known, the fracture threshold can be correctly estimated (**Fig. 10a**). It was observed that the Klesnil-Lucas model contemplates an initial curve in the growth ratio, fitting the slow growth behavior and the controlled growth region II. **Fig. 10b** compares the estimated number of cycles between the models and although the detailed progress of the crack versus cycling is not recorded, it is known that 498900 cycles were necessary in the experimental test (Zhao et al., 2008). In general, Paris-Erdogan underestimates the lifetime of the element by predicting higher-than-actual growth rates at the beginning of propagation, which implies that using Paris-Erdogan (Paris & Erdogan, 1963) to simulate full growth is a very conservative approach. Moreover, Klesnil-Lucas estimates the number of elapsed cycles with a low percentage error (**Table 4**).

Table 4. Percentage error in the number of cycles for 7075 – T651 aluminum alloy simulation.

Experimental elapsed cycles	Paris - Erdogan	Error [%]	Klesnil - Lucas	Error [%]
498900	246682	50.55	513262	2.88

Considering that the fracture threshold refers to the variation of the stress intensity factor for a growth rate of 10^{-10} m/cycle and since the values presented in **Fig. 10** start from approximately 4.5×10^{-9} m/cycle, the experimental results of Newman (Newman et al., 2014) were used to conclude that the behavior presented by Zhao (Zhao et al., 2008) only covers region II of crack growth and still does not give a clear indication of the actual fracture threshold of the material. The 7075-T651 alloy presents a curvature in the crack growth behavior between 3×6 MPa$\sqrt{m}$ even in region II, so the fracture threshold $\Delta K^*_{th} = 4.58$ MPa$\sqrt{m}$ works as an apparent value that provides good results only when $\Delta K > 5$ MPa$\sqrt{m}$. The real fracture threshold is $\Delta K_{th} = 2.05$ MPa$\sqrt{m}$, using this value and with a fracture toughness of $K_{Ic} = 54$ MPa$\sqrt{m}$ the results in **Fig. 11** were computed for the entire crack growth in the three propagation regions and are overlapped with the experimental data reported by Newman (Newman et al., 2014). The three models show similar results in region II, that is, closely resemble the Paris-Erdogan line for medium values of ΔK $\left(4 \leq \Delta K \leq 10 \text{ MPa}\sqrt{m}\right)$.

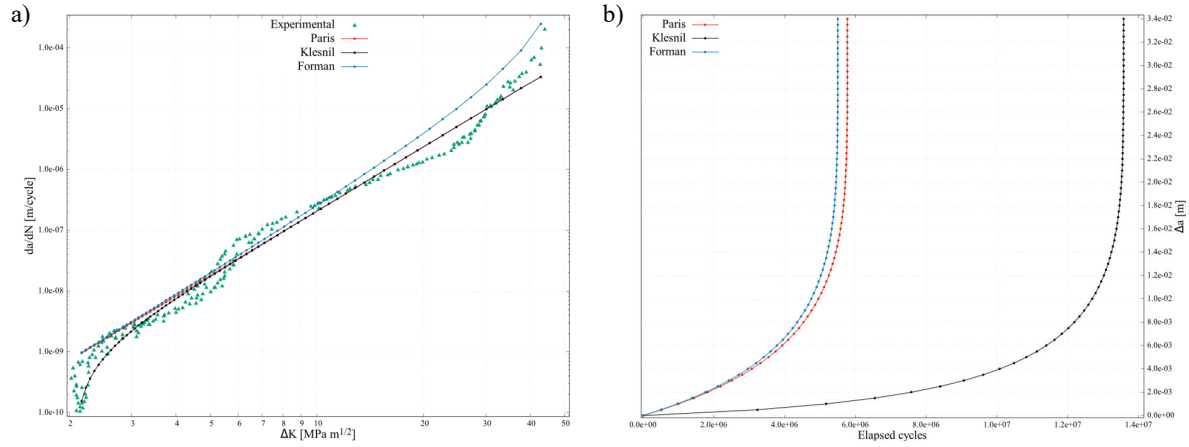

Fig. 11. Fatigue crack growth simulation of 7075-T651 aluminum alloy. a) Crack growth plot, b) Crack size vs. number of cycles.

Since the slow crack growth typical of region *I* is the most cycle demanding, the Klesnil-Lucas model is considered suitable for modeling crack growth involving all 3 regions. Klesnil-Lucas (Klesnil & Lukáš, 1972) is recommended only when the experimental behavior of the material is well known, and the fracture threshold can be accurately calculated. A small variation in this parameter drastically changes the number of cycles. Note in **Fig. 11b** the difference in the number of cycles estimated between Paris-Erdogan and Forman; this variation represents the small error introduced by not considering the behavior of region III in the analysis, whereas if region I, represented by Klesnil-Lucas, is not considered, less than half of the element lifetime is estimated. Forman is recognized as the most conservative of the models analyzed. As a result, it is widely used in simulations and integrity analysis, Krscanski (Krscanski & Brnic, 2020) used the standard Forman model to estimate the lifetime of metallic elements with FEM virtual crack closure technique and Cheng (Cheng & Chen, 2017) applied the Forman model in pipeline carbon steels to various regions of the fatigue crack growth plot, as the shape changes due to hydrogen embrittlement.

3.4 Perforated Plate (PP)

Finally, an application case is discussed, due to the loading conditions, geometry and spatial configuration of the crack, the two stress intensity factors (K_I and K_{II}) are significantly present at the onset of propagation. The maximum tangential stress criterion was validated with the experimental path obtained by Boljanovic (Boljanović & Maksimović, 2011) and with the finite element simulation with NASTRAN (Autodesk Inc., California, USA) performed by this author. Sajith (Sajith et al., 2019) approaches the same problem with FRANC2D (Cornell University, USA) and his results were also used for trajectory validation and predictions through Paris-Erdogan model. Crack growth was modeled in aluminum alloy 2024-T3 with mechanical properties E = 71200 Mpa, v = 0.33 and with the dimensions of **Fig. 12**. The crack emerges from a hole, with an angle of 45° and initial length a_i = 2 mm. The traction applied at both ends is t = 20.8 MPa with a load ratio R = 0.1, however, regarding the boundary conditions, the bottom face of the specimen was fixed, and the traction was only applied to the top face. Growth was simulated up to a final size a_f = 18.2 mm, by 162 increments of 0.1 mm each.

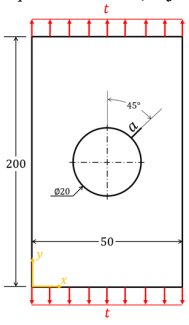

Fig. 12. Geometry and boundary conditions for PP simulation, dimensions in mm.

Fig. 13 shows the results for the stress intensity factors obtained during propagation. At the onset of growth, due to the crack orientation, there is a mixed mode of loading, which implies that the crack propagates with an initial angle of - 43° relative to the local coordinate system (**Fig. 14**). This angle estimated by the maximum tangential stress criterion agrees with the - 42° obtained by Boljanovic (Boljanović & Maksimović, 2011).

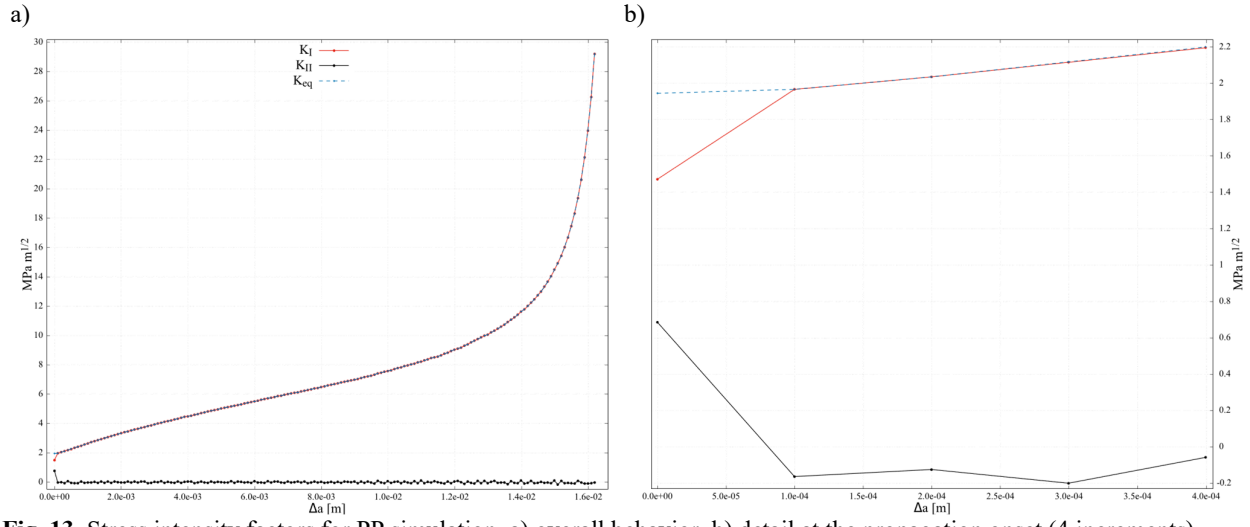

Fig. 13. Stress intensity factors for PP simulation. a) overall behavior, b) detail at the propagation onset (4 increments).

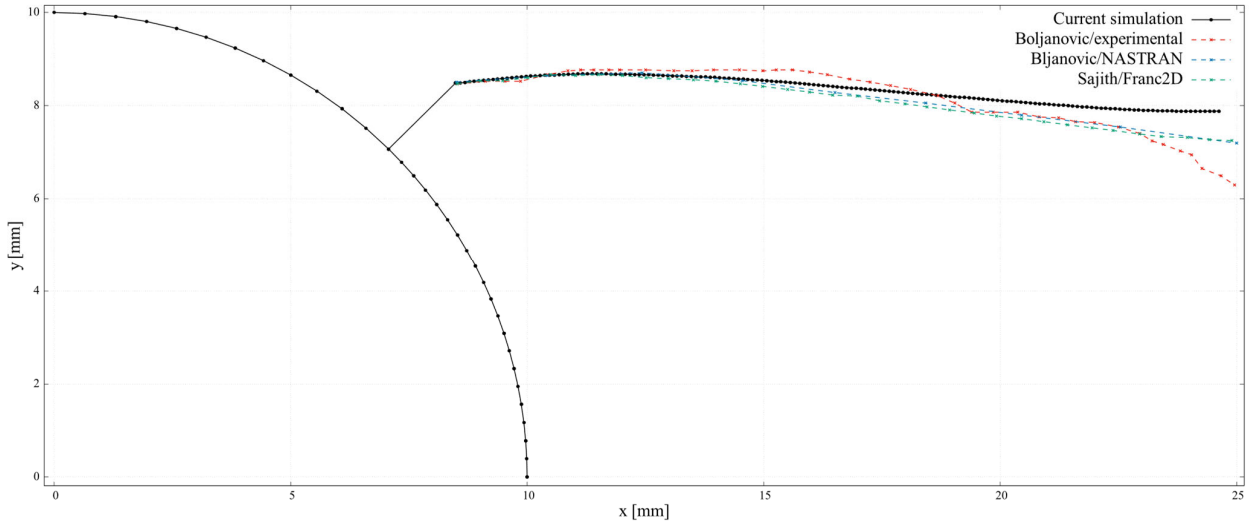

Fig. 14. Crack propagation path for PP simulation. Model agreement with the references, two by the finite element method and one experimental.

After the first step, the stress intensity factor K_{II} cancels out completely while K_I increases with crack size, this behavior leads to the trajectory being perpendicular to the applied load (**Fig. 14**), i.e., in a mode I fracture. To validate the Paris model implementation and calculate an error in the number of cycles estimation, parameters $C = 2.22\times 10^{-10}$ and $m = 3.545$ were used as in the reference (Boljanović & Maksimović, 2011). **Fig. 15** shows the comparison in the number of cycles between the implemented Paris model and the finite element reference.

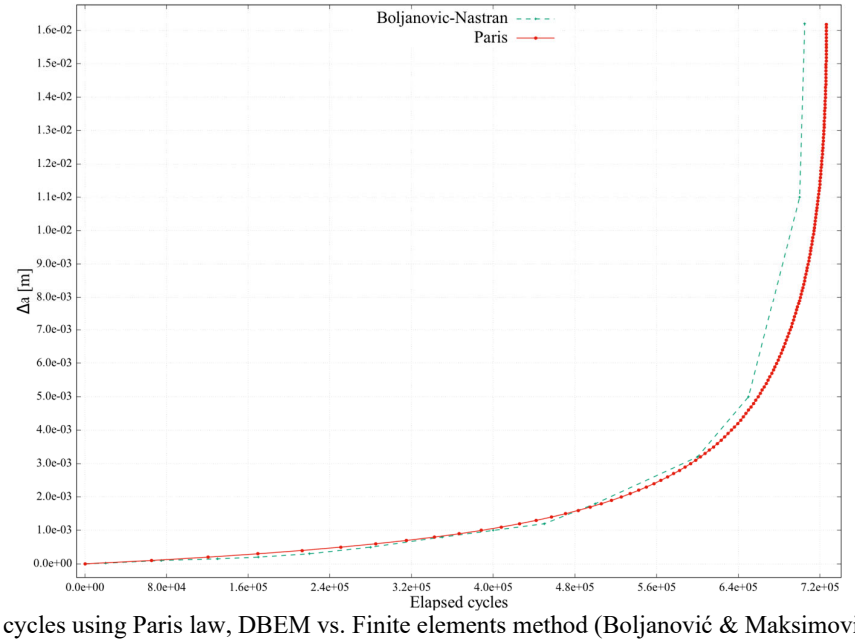

Fig. 15. Number of cycles using Paris law, DBEM vs. Finite elements method (Boljanović & Maksimović, 2011).

A percentage error of 3% was calculated between the estimated cycles (**Table 5**), this variation might be due to the method used for the calculation of the effective stress intensity factor. Boljanovic uses a polynomial expression based on previous simulations, in contrast to the present study which uses Tanaka's model (10) based on Lardner's dislocation theory (Lardner, 1968).

Table 5. Percentage error in the number of cycles for PP simulation.

FEM / Nastran	DBEM	Error [%]
705000	726223	3.01

Although the number of cycles was validated with another computational simulation, it is important to verify that, with these conditions, the crack growth only takes place in the stable propagation region and can be accurately simulated with Paris-Erdogan.

4. Conclusions

Several study cases of the general cracked body problem have been analyzed under mixed boundary conditions using the dual two-dimensional (2D) boundary element method, which is an effective approach for the proposed analysis. Each growth model has the problem constraint of not being able to successfully represent one or more of the crack growth zones. The Paris model can only consider a straight line corresponding to the stable crack growth behavior; Klesnil includes I and II regions without being able to predict values for fast and uncontrolled crack growth, while Forman models the fast crack growth region and part of the stable propagation.

Based on the simulations performed, it was deduced that region III of crack growth occurs in a few load cycles, less than 2% of the total, and for this reason it can be disregarded in the estimation of component lifetime. Moreover, the region I demands the largest number of cycles in the entire propagation, about 50% of the total, and therefore the Klesnil-Lukas model becomes the most suitable for estimating the growth ratios and the total number of elapsed cycles; however, special caution must be taken with the fracture threshold; a small variation in this parameter of 5% is reflected in errors of 25% in the estimation of the number of cycles. In the absence of a known fracture threshold, a traditional crack growth analysis using the Paris model is recommended.

Declaration of competing interest

The authors declare that they have no known competing financial interests or personal relationships that could have appeared to influence the work reported in this paper.

References

Aliabadi, M. H. (1997). Boundary Element Formulations in Fracture Mechanics. *Applied Mechanics Reviews*, *50*(2), 83–96. https://doi.org/10.1115/1.3101690

Amsterdam, E., Willem E. Wiegman, J., Nawijn, M., & De Hosson, J. T. M. (2023). On the strain energy release rate and fatigue crack growth rate in metallic alloys. *Engineering Fracture Mechanics*, *286*, 109292. https://doi.org/10.1016/J.ENGFRACMECH.2023.109292

ASTM. (2023). *Standard Test Method for Measurement of Fatigue Crack Growth Rates, E647 - 23*. https://doi.org/10.1520/E0647-23A

Balderrama, R., Cisilino, A. P., & Martinez, M. (2006). Boundary Element Method Analysis of Three-Dimensional Thermoelastic Fracture Problems Using the Energy Domain Integral. *Journal of Applied Mechanics*, *73*(6), 959–969. https://doi.org/10.1115/1.2173287

Bassindale, C., Wang, X., Tyson, W. R., & Xu, S. (2018). Numerical verification of stress intensity factor solution for clamped single edge notched tension (SENT) specimens. *Fatigue & Fracture of Engineering Materials & Structures*, *41*(2), 494–499. https://doi.org/10.1111/FFE.12700

Boljanović, S., & Maksimović, S. (2011). Analysis of the crack growth propagation process under mixed-mode loading. *Engineering Fracture Mechanics*, *78*(8), 1565–1576. https://doi.org/10.1016/J.ENGFRACMECH.2011.02.003

Cheng, A., & Chen, N. Z. (2017). Fatigue crack growth modelling for pipeline carbon steels under gaseous hydrogen conditions. *International Journal of Fatigue*, *96*, 152–161. https://doi.org/10.1016/J.IJFATIGUE.2016.11.029

Citarella, R., Giannella, V., Vivo, E., & Mazzeo, M. (2016). FEM-DBEM approach for crack propagation in a low pressure aeroengine turbine vane segment. *Theoretical and Applied Fracture Mechanics*, *86*, 143–152. https://doi.org/10.1016/J.TAFMEC.2016.05.004

Díaz, J. G., & Freire, J. L. de F. (2022). LEFM crack path models evaluation under proportional and non-proportional load in low carbon steels using digital image correlation data. *International Journal of Fatigue*, *156*, 106687. https://doi.org/10.1016/J.IJFATIGUE.2021.106687

Forman, R. G., Kearney, V. E., & Engle, R. M. (1967). Numerical Analysis of Crack Propagation in Cyclic-Loaded Structures. *Journal of Basic Engineering*, *89*(3), 459–463. https://doi.org/10.1115/1.3609637

Gdoutos, E. E. (1990). Linear elastic stress field in cracked bodies. *Fracture Mechanics Criteria and Applications*, 15–75. https://doi.org/10.1007/978-94-009-1956-3_2

Gómez, E., Díaz, J., Mantilla, J., Bohorquez, O., & Martínez, M. (2024). Experimental and Numerical Evaluation of Equivalent Stress Intensity Factor Models under Mixed-Mode (I+II) Loading. *Infrastructures 2024, Vol. 9, Page 45*, *9*(3), 45. https://doi.org/10.3390/INFRASTRUCTURES9030045

Kats, B. A., & Katz, D. B. (2019). Cauchy–Hadamard integral with applications. *Monatshefte Für Mathematik 2019 189:4*, *189*(4), 683–689. https://doi.org/10.1007/S00605-019-01263-Z

Klesnil, M., & Lukáš, P. (1972). Influence of strength and stress history on growth and stabilisation of fatigue cracks. *Engineering Fracture Mechanics*, *4*(1), 77–92. https://doi.org/10.1016/0013-7944(72)90078-1

Koko, A., Earp, P., Wigger, T., Tong, J., & Marrow, T. J. (2020). J-integral analysis: An EDXD and DIC comparative study for a fatigue crack. *International Journal of Fatigue*, *134*, 105474. https://doi.org/10.1016/J.IJFATIGUE.2020.105474

Krscanski, S., & Brnic, J. (2020). Prediction of fatigue crack growth in metallic specimens under constant amplitude loading using virtual crack closure and forman model. *Metals*, *10*(7), 1–14. https://doi.org/10.3390/MET10070977

Lardner, R. W. (1968). A dislocation model for fatigue crack growth in metals. *The Philosophical Magazine: A Journal of Theoretical Experimental and Applied Physics*, *17*(145), 71–82. https://doi.org/10.1080/14786436808218181

Leite, P. G. P., & Gomes, G. (2019). Numerical simulation of fatigue crack propagation in mixed-mode (I+II) using the program BemCracker2D. *International Journal of Structural Integrity*, *10*(4), 497–514. https://doi.org/10.1108/IJSI-04-2018-0022

Liu, C., Li, B., Cai, Y., & Chen, X. (2020). Fatigue crack propagation behaviour of pressurised elbow pipes under cyclic bending. *Thin-Walled Structures*, *154*, 106882. https://doi.org/10.1016/J.TWS.2020.106882

Machniewicz, T. (2013). Fatigue crack growth prediction models for metallic materials. *Fatigue & Fracture of Engineering Materials & Structures*, *36*(4), 293–307. https://doi.org/10.1111/J.1460-2695.2012.01721.X

Malíková, L., Veselý, V., & Seitl, S. (2016). Crack propagation direction in a mixed mode geometry estimated via multi-parameter fracture criteria. *International Journal of Fatigue*, *89*, 99–107. https://doi.org/10.1016/J.IJFATIGUE.2016.01.010

Mantilla, J., Poveda, D., & Martínez, M. (2021). Estimation of the Stress Intensity Factor in a Wedge Splitting Test Under Static Load Using the Finite Elements Method. *Respuestas*, *26*(1), 53–61. https://doi.org/10.22463/0122820X.1934

Moore, P., & Pisarski, H. (2017). SENT testing standard BS 8571 and its ongoing development. *International Journal of Pressure Vessels and Piping*, *156*, 2–7. https://doi.org/10.1016/J.IJPVP.2017.05.011

Mukherjee, A., Ghosh, M., Mondal, K., Venkitanarayanan, P., Moon, A. P., & Varshney, A. (2015). Study of mechanical properties, microstructures and corrosion behavior of al 7075 t651 alloy with varying strain rate. *IOP Conference Series: Materials Science and Engineering*, *75*(1), 012031. https://doi.org/10.1088/1757-899X/75/1/012031

Newman, J. C., Anagnostou, E. L., & Rusk, D. (2014). Fatigue and crack-growth analyses on 7075-T651 aluminum alloy coupons under constant- and variable-amplitude loading. *International Journal of Fatigue*, *62*, 133–143. https://doi.org/10.1016/J.IJFATIGUE.2013.04.020

Paris, P., & Erdogan, F. (1963). A Critical Analysis of Crack Propagation Laws. *Journal of Basic Engineering*, *85*(4), 528–533. https://doi.org/10.1115/1.3656900

Peixoto, R. G., Borges, B., Fonseca, F., & Guerra Peixoto, R. (2023). *Direct evaluation of J-Integrals by Gauss-Legendre quadrature in the Dual Boundary Element Method*. https://doi.org/10.21203/RS.3.RS-3168091/V1

Portela, A., Aliabadi, M. H., & Rooke, D. P. (1993). Dual boundary element incremental analysis of crack propagation. *Computers & Structures*, *46*(2), 237–247. https://doi.org/10.1016/0045-7949(93)90189-K

Price, R. J., & Trevelyan, J. (2014a). Boundary element simulation of fatigue crack growth in multi-site damage. *Engineering Analysis with Boundary Elements*, *43*, 67–75. https://doi.org/10.1016/J.ENGANABOUND.2014.03.002

Price, R. J., & Trevelyan, J. (2014b). Boundary element simulation of fatigue crack growth in multi-site damage. *Engineering Analysis with Boundary Elements*, *43*, 67–75. https://doi.org/10.1016/J.ENGANABOUND.2014.03.002

Rice, J. R. (1968). A Path Independent Integral and the Approximate Analysis of Strain Concentration by Notches and Cracks. *Journal of Applied Mechanics*, *35*(2), 379–386. https://doi.org/10.1115/1.3601206

Sajith, S., Murthy, K. S. R. K., & Robi, P. S. (2019). Mixed mode fatigue crack growth studies of crack emanating from circular hole. *AIP Conference Proceedings*, *2200*(1), 020041. https://doi.org/10.1063/1.5141211

Sajith, S., Shukla, S. S., Murthy, K. S. R. K., & Robi, P. S. (2020). Mixed mode fatigue crack growth studies in AISI 316 stainless steel. *European Journal of Mechanics - A/Solids*, *80*, 103898. https://doi.org/10.1016/J.EUROMECHSOL.2019.103898

Sajuri, Z., Alang, N. A., Razak, N. A., & Aziman, M. A. (2011). Fracture Toughness and Fatigue Crack Growth Behavior of Rail Track Material. *Key Engineering Materials*, *462–463*, 1109–1114. https://doi.org/10.4028/WWW.SCIENTIFIC.NET/KEM.462-463.1109

Santana, E., & Portela, A. (2016a). Dual boundary element analysis of fatigue crack growth, interaction and linkup. *Engineering Analysis with Boundary Elements*, *64*, 176–195. https://doi.org/10.1016/J.ENGANABOUND.2015.12.002

Santana, E., & Portela, A. (2016b). Dual boundary element analysis of fatigue crack growth, interaction and linkup. *Engineering Analysis with Boundary Elements*, *64*, 176–195. https://doi.org/10.1016/J.ENGANABOUND.2015.12.002

Sedmak, A. (2018). Computational fracture mechanics: An overview from early efforts to recent achievements. *Fatigue & Fracture of Engineering Materials & Structures*, *41*(12), 2438–2474. https://doi.org/10.1111/FFE.12912

Shen, G., Gianetto, J., & Tyson, W. (2009). Measurement of J-R Curves Using Single-Specimen Technique On Clamped SE(T) Specimens. *The Nineteenth International Offshore and Polar Engineering Conference*.

Shlyannikov, V., Yarullin, R., Yakovlev, M., Giannella, V., & Citarella, R. (2021). Mixed-mode crack growth simulation in aviation engine compressor disk. *Engineering Fracture Mechanics*, *246*, 107617. https://doi.org/10.1016/J.ENGFRACMECH.2021.107617

Shukla, S. S., & Murthy, K. S. R. K. (2023). A study on the effect of different Paris constants in mixed mode (I/II) fatigue life prediction in Al 7075-T6 alloy. *International Journal of Fatigue*, *176*, 107895. https://doi.org/10.1016/J.IJFATIGUE.2023.107895

Singh, A., Tang, L., Dao, M., Lu, L., & Suresh, S. (2011). Fracture toughness and fatigue crack growth characteristics of nanotwinned copper. *Acta Materialia*, *59*(6), 2437–2446. https://doi.org/10.1016/J.ACTAMAT.2010.12.043

Tanaka, K. (1974). Fatigue crack propagation from a crack inclined to the cyclic tensile axis. *Engineering Fracture Mechanics*, *6*(3), 493–507. https://doi.org/10.1016/0013-7944(74)90007-1

Tanaka, K. (1983). The cyclic J-integral as a criterion for fatigue crack growth. *International Journal of Fracture*, *22*(2), 91–104. https://doi.org/10.1007/BF00942715/METRICS

Vaidya, W. V., Horstmann, M., Angamuthu, K., & Koçak, M. (2010). Utilising CODmax as an indirect fatigue crack length measurement parameter for M(T) specimens of an airframe aluminium alloy AA6056. *Materialpruefung/Materials Testing*, *52*(11–12), 771–777. https://doi.org/10.3139/120.110185

Wang, C., Pereira, K., Wang, D., Zinovev, A., Terentyev, D., & Abdel Wahab, M. (2023). Fretting fatigue crack propagation under out-of-phase loading conditions using extended maximum tangential stress criterion. *Tribology International*, *187*, 108738. https://doi.org/10.1016/J.TRIBOINT.2023.108738

Wen, P., & Aliabadi, M. (2012). Dual Boundary Element Method for Modelling Curved Crack Paths. *International Journal of Fracture* , *176*, 127–133. https://doi.org/10.1007/s10704-012-9719-x

Xu, M., Liu, Y., & Yuan, H. (2022). Characterization of crack-tip fields for elastoplastic fatigue crack growth Part I: Analysis of the ΔJ-integral. *Engineering Fracture Mechanics*, *275*, 108847. https://doi.org/10.1016/J.ENGFRACMECH.2022.108847

Zhao, T., Zhang, J., & Jiang, Y. (2008). A study of fatigue crack growth of 7075-T651 aluminum alloy. *International Journal of Fatigue*, *30*(7), 1169–1180. https://doi.org/10.1016/J.IJFATIGUE.2007.09.006

Zhu, X. K. (2017). Full-range stress intensity factor solutions for clamped SENT specimens. *International Journal of Pressure Vessels and Piping*, *149*, 1–13. https://doi.org/10.1016/J.IJPVP.2016.11.004